Environ. Sci. Technol. **2008,** *42,* 308–314

Enhanced Photocatalytic Degradation of Dye Pollutants under Visible Irradiation on Al(III)-Modified TiO_2: Structure, Interaction, and Interfacial Electron Transfer

DAN ZHAO,[†] CHUNCHENG CHEN,*[,†] YIFENG WANG,[†] WANHONG MA,[†] JINCAI ZHAO,*[,†] TIJANA RAJH,[‡] AND LING ZANG[§]

Beijing National Laboratory for Molecular Sciences, Key Laboratory of Photochemistry, Institute of Chemistry, Chinese Academy of Sciences (CAS), Beijing 100080, China, Chemistry Division, Materials Science Division, Argonne National Laboratory, Argonne, Illinois 60439, and Department of Chemistry and Biochemistry, Southern Illinois University, Carbondale, Illinois 62901

Received July 18, 2007. Revised manuscript received September 24, 2007. Accepted October 3, 2007.

Aluminum(III)-modified TiO_2 was prepared by sol–gel process via a sudden gelating method. The structure of the modified material and the local environment of aluminum were investigated using X-ray diffraction, HRTEM, XPS, ^{27}Al MAS NMR, and ξ-potential measurements. The effect of the aluminum modification on interaction between the dye and photocatalyst, the interfacial electron transfer process, and thereby the degradation of dye pollutants under visible irradiation were also examined by FTIR spectra and UV–vis diffuse reflectance spectra. It was found that, rather than incorporating into the crystal lattice of TiO_2, the aluminum forms an overlayer of Al_2O_3 on the surface of TiO_2, interfaced with Ti−O−Al bonds. It is interesting that the carboxylate-containing dyes such as Rhodamine B (RhB) adsorb preferentially on the Al_2O_3, rather than the Ti(IV) sites on the surface of TiO_2. The photodegradation rate observed for RhB is nearly 5-fold faster than that obtained in the pristine TiO_2 system. The photodegradation of dyes on the aluminum(III)-modified photocatalyst is of great dependence on the structure and anchoring group of the dyes. Structure with carboxylate as anchoring group and amino group as electron donor is favorable for degradation. The mechanistic details are discussed on the basis of experimental results.

Introduction

Numerous studies have been reported on the photocatalytic reaction mediated by TiO_2 under ultraviolet irradiation. One obstacle toward its practical application is that photocatalytic processes can only be activated by ultraviolet light, which accounts for only about 4% of the incoming solar energy. To extend the visible response of this material, great efforts have been made to modify the TiO_2-based catalysts. In recent years, our group and others have reported the visible-light-induced degradation and mineralization of dye pollutants (*1–6*), which cause a great deal of environmental problems around the world (*7–9*). In these systems, the dye pollutants, rather than the TiO_2 photocatalyst, are subject to the visible light excitation. The excited dye molecule transfers an electron into the conduction band of TiO_2, leading to formation of a cationic radical of the dye. The injected electron then reacts with the dioxygen adsorbed on the surface of TiO_2, and generates a series of active oxygen radicals such as O_2•-, •OH, and H_2O_2. The subsequent radical chain reactions lead to the degradation and mineralization of the dye pollutants.

Upon modification with certain dopants, the energy band structure and surface properties of TiO_2 can feasibly be tuned. As a result, the charge separation, the chemical interaction between the organic compounds and TiO_2, and the radical chain reactions can be changed. Recently, modification by aluminum(III) and Al_2O_3 has received increasing attention, since it demonstrates enhancement in both the photocatalytic activity under UV irradiation and solar energy conversion efficiency of TiO_2 (*10–16*). For example, the mineralization of maleic acid was observed to be greatly enhanced by the preadsorption of aluminum(III) on the surface of TiO_2 (*10*). The mixed oxides TiO_2/Al_2O_3 prepared by Anderson and Bard using sol–gel methods showed improved activity for the photocatalytic decomposition of salicylic acid under UV irradiation (*12*). It was also reported that the efficiency of dye-sensitized solar cell was improved by 35% after modifying the TiO_2 with insulating Al_2O_3, which forms a blocking layer between the dye sensitizer and the TiO_2 particles (*13–16*). In these systems, the electron injection from the excited dye molecule into the conduction band of TiO_2 can occur by tunneling through the very thin insulating Al_2O_3 layer. Consequently, the charge separation between the injected electrons and the dye cation radicals is improved, since the charge recombination is significantly blocked by the insulating layer of Al_2O_3.

Since the photodegradation of dye under visible irradiation is initiated by the interfacial electron injection from the excited dye molecule into the TiO_2 catalyst, the overall photocatalytic efficiency should be largely dependent on the electron injection and recombination between the dye and TiO_2. Such charge transfer processes are generally considered using Marcus nonadiabatic electron-transfer theory (*15, 17–19*), for which the rates of both electron injection and recombination depend upon the electronic coupling between the donor and acceptor states besides the relative energy levels of these states. It has been reported that the injection and recombination kinetics follow exponential dependence upon spatial separation of the donor and acceptor (*20, 21*). Thus the interfacial interaction (with regard to both binding modes and sites) between the dye and TiO_2 can potentially alter the photocatalytic kinetics and degradation efficiency. However, such interfacial interaction and the effect on photocatalysis have not yet been systematically explored for the Al_2O_3 modified TiO_2.

In this study, we extend the use of aluminum(III)-modified TiO_2 into photocatalytic degradation of dye pollutants under visible irradiation. The research was aimed to clarify (1) the efficiency of the modified photocatalyst for the degradation of dye pollutants under visible irradiation; (2) the chemical state of aluminum and its effect on surface properties of TiO_2; (3) the interaction character between the dye and photocatalyst in the TiO_2 and aluminum(III)-modified TiO_2 systems, and (4) the mechanism of catalytic enhancement of photodegradation of dye pollutants under visible irradiation.

* Corresponding author fax: 86-10-8261-6495; e-mail: jczhao@iccas.ac.cn.
[†] Chinese Academy of Sciences.
[‡] Argonne National Laboratory.
[§] Southern Illinois University.

10.1021/es071770e CCC: $40.75
Published on Web 11/27/2007

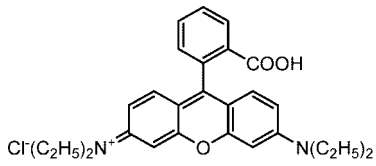

Rhodamine B (RhB)

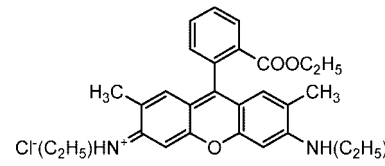

Rhodamine 6G (Rh6G)

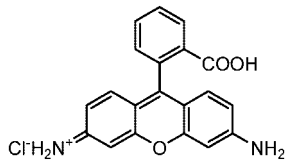

Rhodamine 101 (R101)

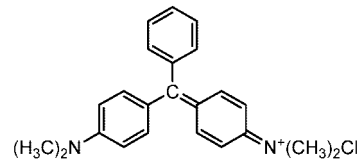

Malachite Green (MG)

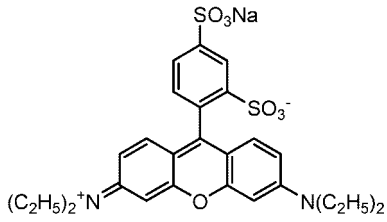

Sulforhodamine B (SRB)

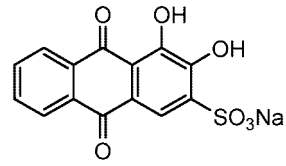

Alizarin red (AR)

Experimental Section

Materials. Aluminum isopropoxide (99.99+%) was purchased from Aldrich. Titanium isopropoxide (98%) was obtained from Acros. Rhodamine-B (RhB), Rhodamine 6G (R6G), Rhodamine 101(R101), and Sulforhodamine B (SRB) dyes were of laser grade quality. The dyes malachite green (MG) and alizarin red (AR) were of analytical reagent grade. The structures of the dyes used in the photodegradation reactions are shown below. Deionized and doubly distilled water was used throughout this study. The pH of the solutions was adjusted with dilute aqueous solutions of $HClO_4$ and NaOH.

Photocatalyst Preparation. The photocatalysts were prepared based on a sol–gel method starting from alkoxides precursors (*22*). Titanium isopropoxide was dissolved in 2-propanol at a volume ratio of 1.5:8.5, followed by addition of appropriate amount of aluminum isopropoxide to obtain Al/Ti atomic ratios of 0, 0.03, 0.05, 0.10, 0.15, and 0.20. After ultrasonic mixing, the alkoxide solution was added dropwise to 200 mL of 0.3 M nitric acid aqueous solution in an ice/water bath under vigorous stirring to form a transparent, homogeneous mixed solution of Al and Ti precursors. Ammonia solution (3.0 M) was then added to adjust the pH of the solution to around 9. After aging for 2 h, the white gel thus formed was separated by centrifugation and washed thoroughly by water to remove the impurity. The gel was then dried at 80 °C, followed by sintering at 430 °C for 3 h. Before use in the photodegradation reaction, the catalysts were washed thoroughly with water again and dried at 100 °C under vacuum overnight.

Structural Characterization. Of all the aluminum(III)-modified TiO_2 catalysts prepared, the one with Al/Ti ratio of 0.10 exhibited the highest activity for the photodegradation of dyes. The structure of this catalyst, termed as TiO_2(0.10Al), was characterized in detail to clarify the mechanism underlying the enhancement in photocatalytic activity. X-ray diffraction (XRD) measurements were performed on a Regaku D/Max-2500 diffractometer with Cu Kα radiation (1.5406 Å). A high-resolution transmission electron microscope (HRTEM) (Philips CM200 FEG TEM at 200 kV) was used to image the morphology and surface structure of the catalyst particles. X-ray photoelectron spectroscopy (XPS) data were recorded with an ESCA laboratory 220i-XL spectrometer using Al Kα (1486.6 eV) X-ray source. To eliminate charge effect, all the spectra were calibrated to the binding energy of adventitious C 1s peak at 284.8 eV. To characterize the local structure around aluminum in the samples, solid-state ^{27}Al magic-angle spinning (MAS) NMR spectra were measured on a spectrometer (model AV 300, Bruker Instruments) operating at 78.20 MHz and at a spinning rate of 8 kHz. A Zetasizer 2000 (United Kingdom, Malvern Co.) was employed to determine ξ- potentials of the photocatalysts. For these measurements, the suspensions containing 0.1 g/L TiO_2 were used, and the pH was adjusted between pH 2.5 and 11.0 using dilute NaOH and HNO_3 solutions.

The samples for FTIR experiments were prepared as follows: the unmodified TiO_2 and aluminum(III)-modified TiO_2 were dispersed in a 2 mM solution of RhB to reach the adsorption equilibrium, followed by centrifugation to separate the solid sample. The RhB adsorbed catalysts thus prepared were rinsed thoroughly with water to remove the physically adsorbed dye, and then dried in air at 35 °C. All the processes were carried out in dark to prevent photodegradation of the adsorbed dyes. The infrared spectra were obtained on a TENSOR 27 FTIR spectrometer (Bruker) in the diffuse reflectance mode. The blank photocatalysts, pretreated under the same conditions but in the absence of the dye, were used as the background reference (*23*). Hitachi U-3010 was used to record the UV–vis diffuse reflectance absorption spectra. The steady-state fluorescence emission measurements were performed on the Hitachi F-4500 spectrometer.

Photodegradation of Dyes. The light source used was a 500-W halogen lamp (Institute of Electric Light source, Beijing, China) positioned inside a cylindrical Pyrex reactor and surrounded by a circulating water jacket for cooling. To ensure illumination by only visible light, a cutoff filter was placed outside the Pyrex jacket to completely eliminate any radiation at wavelength below 450 nm. Fifty mL of an aqueous

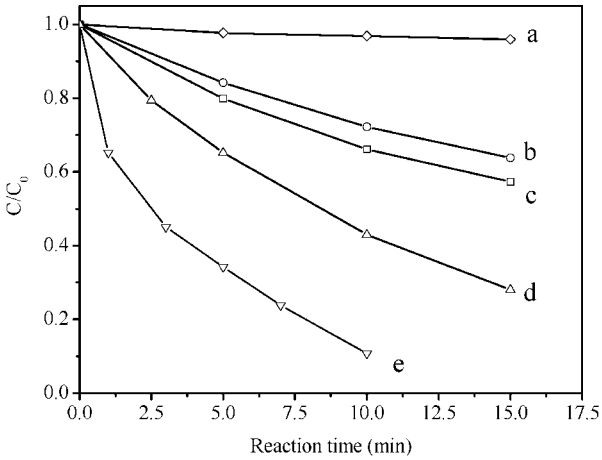

FIGURE 1. Temporal course of the photodegradation of RhB (2.0×10^{-5} M; 50 mL) at pH 2.5 in aqueous dispersions containing 25 mg of catalysts under visible irradiation: (a) TiO_2(0.10Al) in the dark, (b) P25, (c) prepared pure TiO_2, (d) TiO_2(0.05Al) and (e) TiO_2(0.10Al).

solution containing given concentration of dyes and certain amount of catalyst powders was placed in a Pyrex vessel. Prior to irradiation, the suspensions were magnetically stirred in the dark for ca. 60 min to ensure the establishment of an adsorption/desorption equilibrium. At a given time, 3 mL aliquots were collected, centrifuged, and then filtered through a Millipore filter (pore size 0.2 μm) to remove the solid catalyst particles. The filtrate was then subjected to analysis of the concentration and the intermediates of RhB using a UV–vis spectrophotometer (Lambda Bio-20) and high-performance liquid chromatography (HPLC) (Dionex P580 pump and UVD340S diode array detector).

Results and Discussion

Photocatalytic Activity for the Degradation of Dye Pollutants. Figure 1 compares the kinetics of the photodegradation of dye RhB under visible irradiation in the presence of different catalysts. No reaction was observed in the presence of TiO_2(0.10Al) in the dark (curve a). Under visible irradiation, all the systems exhibited notable degradation for RhB. The concentration of RhB tended to decrease exponentially with irradiation time, and thus the kinetics was fitted by pseudo-first-order process. The decay rate constant of RhB obtained for the pure TiO_2 catalyst was 0.037 ± 0.003 min^{-1} (curve c). Upon modification with aluminum, the degradation of RhB was markedly enhanced, and the pseudo-first-order kinetic constant increased to 0.084 ± 0.001 min^{-1} and 0.21 ± 0.01 min^{-1} for TiO_2(0.05Al) and TiO_2(0.10Al), respectively (curves d and e). The rate constant for the degradation of RhB in TiO_2(0.10Al) system is nearly 5-fold higher than that obtained for the pure TiO_2 catalyst. In the earlier studies, we noted that RhB (*1*), (*24*) and other *N*-alkylamine-containing dyes (*25–27*) can be photodegraded via two pathways: (i) *N*-dealkylation of the chromophore skeleton, and (ii) cleavage of the whole conjugated chromophore structure. In the present study, the *N*-dealkylation intermediates of RhB during the photodegradation were examined by HPLC method (Supporting Information Figure S1). It seems that the formation and disappearance of all these intermediates are significantly accelerated in the aluminum(III)-modified TiO_2 system compared to the unmodified TiO_2 system. To compare with the common, commercial TiO_2 photocatalyst, the photodegradation in the presence of P25 TiO_2 was also examined, and the rate constant was 0.030 ± 0.001 min^{-1} (curves b). It is evident that all the photocatalysts prepared in this study, including the aluminum-free TiO_2, exhibit higher photocatalytic activity than P25 TiO_2. The stability of

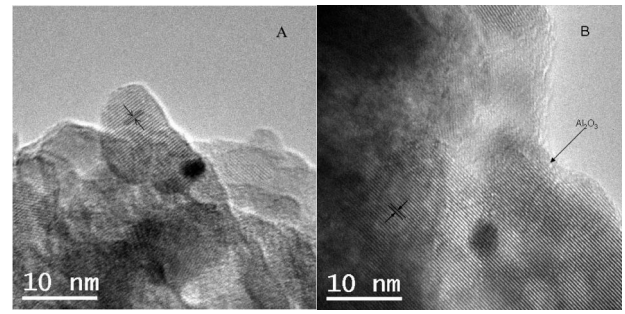

FIGURE 2. HRTEM image of (a) pure TiO_2, and (b) TiO_2(0.10Al).

TiO_2(0.10Al) was examined by repetitive use of the catalyst in six reaction cycles for the degradation of RhB (Supporting Information S2). It was found that the photoactivity of the Al-modified catalyst exhibited no significant loss.

The photodegradation was also performed for other dye molecules, including Rhodamine 6G (R6G), Rhodamine 101 (R101), Sulforhodamine B (SRB), Malachite Geen (MG), and Alizarin red (AR) (results are shown in Table 1). R6G has an ester group instead of carboxylic acid group. However, when binding to the TiO_2, the ester group was reported to transform into carboxylate forms (*28, 29*). Thus, R6G exhibited adsorption and photodegradation similar to that of the RhB on both the pure TiO_2 and aluminum(III)-modified TiO_2. Its adsorption amount increased from 8.24 to 13.32 μmol/g after modification and the kinetics was much faster in TiO_2(0.10Al) system than in pure TiO_2 dispersion. R101 possesses a scaffold structure similar to that of RhB, except that the two diethyl amino groups are replaced by two amino groups in R101. There was also an adsorption enhancement observed for R101 on TiO_2(0.10Al), but the enhancement in degradation rate was not as significant as for RhB, likely due to the weaker electron-donation of R101 (see discussion in Supporting Information, Figure S8). The degradation of sulfonate-containing xanthene dye SRB, cationic triphenylmethane dye MG, and anthraquinone dye AR exhibited no enhancement in the TiO_2(0.10Al) system, although an increased adsorption was found for AR. These results indicate that the dye structure and their anchoring group on the photocatalyst are critical factors that determine the interfacial electron transfer and the degradation of the dye. The carboxylate group seems to be most effective in enhancing the surface binding and thus the photodegradation, consistent with the observation in the photoelectrochemical cells employing carboxylate dyes.

Characteristics of Aluminum Modified Photocatalysts. For the characteristics of photocatalysts, one of the most important issues is the status of the aluminum species within the modified catalyst. In this study, the structural properties of the aluminum-modified catalysts were extensively characterized using various microscopy and spectroscopy techniques, including TEM, XRD, ^{27}Al MAS NMR, XPS, and ξ-potentials, aiming to clarify the chemical status of the aluminum species.

Figure 2A and B show the HRTEM micrographs of the pure TiO_2 and TiO_2(0.10Al), respectively. The image of pure TiO_2 demonstrates the well-crystalline phase of TiO_2 with clear boundary edge. The lattice fringes (with *d* spacing of about 0.35 nm) show that the most frequently observed planes are (101) crystallographic planes of anatase (*30*). After modification by aluminum, the lattice fringes corresponding to (101) crystallographic planes of anatase still remain the most frequently observed planes, but the most notable difference compared to the pure TiO_2 is the emergence of Al_2O_3 layer at the crystallite boundaries of TiO_2 particles. The coating thickness of Al_2O_3 ranges from 0.5 to several nanometers. The average crystallite sizes in both the two catalysts were around 10–20 nm. In addition, there were

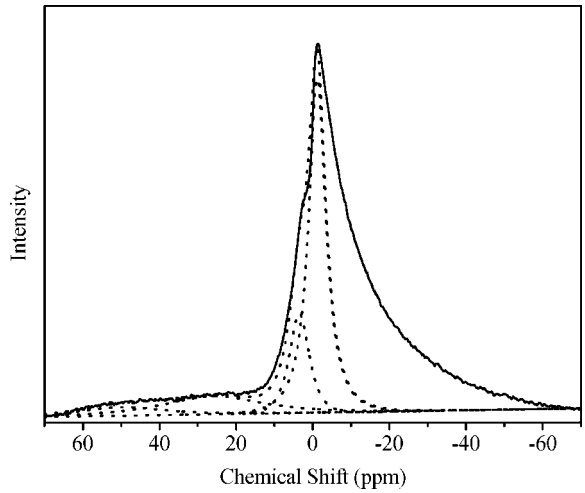

FIGURE 3. ^{27}Al MAS NMR spectrum and its deconvoluted peaks of the TiO_2(0.10Al) sample.

no irregular disturbances in the lattice fringe, suggesting that little Al is weaved into the lattices of the TiO_2 nanoparticles.

Consistent with the TEM observation, the X-ray diffraction patterns (Figure S3) indicate that both the unmodified and modified TiO_2 consist of anatase crystalline phase, and no diffraction peak due to other crystalline phases (for example, rutile TiO_2 or crystalline alumina) were observed. Considering the difference in ion radii between Al^{3+} (0.054nm) and Ti^{4+} (0.061nm) (*31*), there should be some shift in the diffraction peaks of TiO_2, if a large number of Al^{3+} substitute the Ti^{4+} in the bulk crystal lattice to form solid solution. However, all the diffraction peaks of the modified materials showed no shift relative to those obtained for pure TiO_2, confirming further that little aluminum is not incorporated into the crystal phase of TiO_2. Moreover, changing the Al^{3+}/Ti^{4+} ratio from 0 to 0.10 did not result in notable change in crystallite size (Table S1), which is also consistent with the TEM results.

The local environment around the Al atoms in the modified samples was further studied by the ^{27}Al MAS NMR spectra. It has been reported that the chemical shift in ^{27}Al NMR is directly related to the coordination number of the Al^{3+} (*32–34*). The ^{27}Al MAS NMR spectrum and its deconvoluted peaks in the TiO_2(0.10Al) sample are displayed in Figure 3. The shape of the peak at about 0 ppm was asymmetric, probably due to the quadrupolar interaction (*35*). The spectrum could be fitted only on the left onset in multiple Lorentzian lines. It is evident that the intense resonances around 0 ppm for octahedrally coordinated Al^{3+} ions consist of two peaks, located at 4 and −1 ppm. The most pronounced peak located at −1 ppm is assigned to octahedrally coordinated Al^{3+} ions of Al−O−Al type (*32–34*). In SiO_2/Al_2O_3 and SiO_2/TiO_2 systems, the appearance of resonance at lower field relative to normal tetrahedrally coordinated Si was reported, which was assigned to the structure units with several −OTi or −OAl as the neighboring groups around Si. Considering the composition of our aluminum-modified TiO_2 sample, the shoulder peak at lower field (4 ppm) can be attributed to the octahedrally coordinated Al in Al−O−Ti states. The intensity ratio of the signals for Al−O−Ti and Al−O−Al is ca. 0.3, revealing the relative amount of Ti−O−Al and Al−O−Al bonds. Consistently, the XPS spectra (Figure S4) show the ratio of Ti−O−Al bonds (530.9 eV) to Al−O−Al bonds (531.6 eV) to be ca. 0.28. The weak and broad bands observed in the range of 10–60 ppm can be assigned to the tetrahedrally coordinated (50 ppm) and five-coordinated (26 ppm) aluminum.

CHART 1. Proposed interaction modes of carboxylate group with metal (M = Ti or Al in this study)

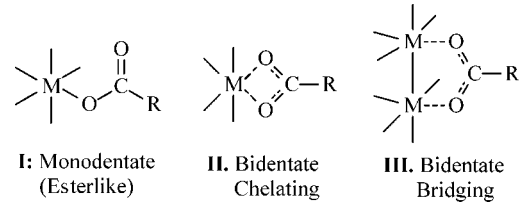

Since Al_2O_3 is a more basic oxide than TiO_2, it is expected that the point of zero charge (pzc) of the modified TiO_2 should shift to higher pH. However, the ξ-potential measurement showed that the pzc (pH 4.9) of the modified TiO_2 became much lower than that of its parent materials (pH 5.8 for pure TiO_2 and pH 8.8 for Al_2O_3) (Figure S5). Since this pzc only reflects the Brönsted acidity on the surface of photocatalyst (*36*), the lower value of pzc may indicate the formation of higher acidic Brönsted sites. It has been observed that the binary metal oxides often display increased acidity over their pure counterparts, which is usually attributed to the charge imbalance caused by doping (*37*). At the interfacial region between Al_2O_3 layer and TiO_2, the excess negative charges will be introduced from the isomorphic substitution of the Ti^{4+} by lower valence cation (Al^{3+}). To satiate the charge balance, the cation (here H^+) must be enriched on the surface of the material, thereby forming the Brönsted acid sites. The formation of Brönsted acid sites can also be explained by the difference in coordination number between the dopant oxide and the host oxide, as suggested by Tanabe's theory (*38*). Hence, the formation of acidic Brönsted sites could be associated to the incorporation of Al^{3+} into the surface of TiO_2, consistent with the existence of Ti−O−Al bonds as indicated by the XPS measurement.

During the preparation of the modified photocatalyst by the sol–gel method, the gel was formed by rapid addition of 3 M ammonia solution into the mixed solution of aluminum and titanium isopropoxides, leading to a final pH of 9. It is expected that both the Al and Ti precursors were simultaneously hydrolyzed into a homogeneous mixture of hydrated oxides of Al and Ti. In the subsequent heat treatment, the amorphous TiO_2 was crystallized first, and such crystallization of TiO_2 expelled the preincorporated Al species to the boundary of TiO_2 crystallites (*39*). The Al_2O_3 species were thus enriched progressively on the surface of TiO_2 particles, eventually forming a thin layer covalently attached to the TiO_2 phase through Ti−O−Al bonds.

Chemical Interaction between Rhodamine B and the Surface of Photocatalyst. Since the interfacial electron transfer from the excited dye to TiO_2 is a critical step toward efficient photocatalysis, the adsorption site and mode of the dye on the surface of TiO_2 are of great importance and have been extensively investigated in both photoelectrochemical solar cells (*40*) and the photodegradation of dye pollutants (*23*, *25*).

The dye used in this study, RhB, contains a carboxylic group, which possesses strong binding ability to the surface of TiO_2 (*41*). Three possible binding modes have been previously proposed for the surface adsorption of carboxylate on metal oxides (Chart 1) (*41–43*): (**I**) the monodentate (esterlike) linkage, (**II**) bidentate chelating, and (**III**) the bidentate bridging. Infrared vibrational spectroscopy usually provides a powerful tool to distinguish these binding modes. Generally, the frequency difference between the antisymmetric and symmetric stretching vibration ($\Delta = \nu_{as} - \nu_a$) of carboxylate group is in the order of Δ(monodentate) > Δ(ionic) ~ Δ(bridging) > Δ(bidentate). For the pure dye, the stretching vibration band of carboxylic group was located at 1697 cm^{-1} (Figure 4, curve a). After coordinating to TiO_2

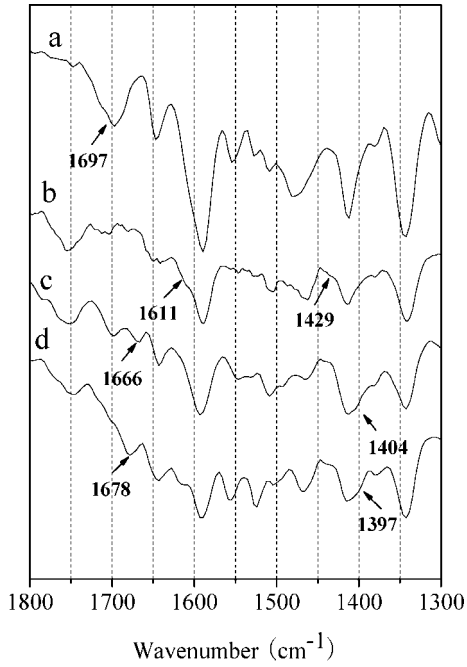

FIGURE 4. FTIR spectra of (a) dye RhB powder, (b) sodium salt of RhB, (c) RhB coordinated to pure TiO_2, and (d) RhB coordinated to TiO_2(0.10Al).

surface, this vibration band splits into two bands (1666 and 1404 cm^{-1}, respectively) (curve c). The band located at 1666 cm^{-1} is ascribed to the antisymmetric stretching vibration of coordinated carboxylate group, while the shoulder band at 1404 cm^{-1} corresponds to the symmetric vibration. For the dye adsorbed on aluminum(III)-modified TiO_2, the splitting of vibration was also observed, and the antisymmetric and symmetric band are located at 1678 and 1397 cm^{-1}, respectively (curve d) (*44*). The fact that the Δ value for RhB adsorbed on the pure TiO_2 (Δ = 262 cm^{-1}) and aluminum(III)-modified TiO_2 (Δ = 281 cm^{-1}) system are much larger than that obtained for the sodium salt of RhB (Δ = 182 cm^{-1}) suggests that the binding mode of RhB on the catalyst was dominantly the monodentate esterlike linkage. It was also found that the frequency of −COO antisymmetric stretch of the dye coordinated on TiO_2(0.10Al) surface (ν_{as} = 1678 cm^{-1}) was 12 cm^{-1} higher than that on pure TiO_2 surface (ν_{as} = 1666 cm^{-1}), while the frequency of −COO symmetric stretch was 7 cm^{-1} lower. Calculation on carboxylate coordination demonstrated that in the form of esterlike linkage, the shift for ν_{as} (COO) to longer wavenumber and ν_s (COO) to shorter wavenumber is dependent on the intensity of interaction. The stronger the interaction between −COO and the metal ion, the larger the frequency shift is (*45*). The larger frequency shift observed for RhB adsorbed on TiO_2(0.10Al) compared to that on pure TiO_2 implies that RhB predominantly adsorbs on the Al_2O_3 phase, since the interaction between −COO and the Al^{3+} site is stronger than that between −COO and the Ti^{4+} sites. This argument is further supported by the larger (compared to that on pure TiO_2) red-shift in diffuse reflectance spectra and the fluorescence emission peaks of the dye adsorbed on TiO_2(0.10Al) (Figure S7). This strong interaction can play a favorable role in the electron injection.

The enhanced adsorption of the dyes on aluminum-modified TiO_2 were observed in the process of photodegradation. Under our experimental conditions (pH 2.5, initial dye concentration 20 μM, photocatalyst 0.5 g/L), the adsorption amount of RhB on aluminum-modified TiO_2 was about 15.6 μmol dye/g photocatalyst, which was much greater than that on pure TiO_2 (5.8 μmol dye/g). The adsorption amount of other dyes, Rh6G and R101, also increased to some extent on aluminum-modified TiO_2. It is known that liquid–solid heterogeneous photocatalysis is an interface-based process. The contact of dye molecules with the surface of catalyst is prerequisite to efficient electron transfer. Therefore the enhanced adsorption of dye will partly contribute to the high photocatalytic activity of aluminum-modified TiO_2.

TABLE 1. Adsorption Amount and Photocatalytic Degradation Rates of Various Dyes on Pure TiO_2 and Aluminum(III)-Modified TiO_2[a]

dyes	adsorption amount (μmol/g)		dye conversion[e] (%)	
	TiO_2	TiO_2(0.10Al)	TiO_2	TiO_2(0.10Al)
Rhodamine B[b]	5.84	15.64	33.87	89.25
Rhodamine 6G[b]	8.24	13.32	9.22	28.49
Rhodamine 101[c]	1.82	7.92	15.01	19.67
Sulforhodamine B[b]	14.2	12.96	36.73	35.88
Malachite Geen[b]	2.64	3.44	8.15	8.52
Alizarin Red[d]	178.2	280.8	12.38	11.14

[a] Catalyst: 0.5 g/L, pH = 2.5. [b] Initial concentration is 2.0 × 10^{-5} M. [c] Initial concentration is 1.6 × 10^{-5} M. [d] 3.0 × 10^{-4}M for AR. [e] Percentage of dye which has been decomposed after 30 min for Rh6G, Rh101, SRB, and AR, 10 min for RhB, and 60 min for SRB irradiation, respectively.

Considering that the photodegradation of dyes under visible irradiation is initiated by the interfacial electron injection from the excited dye molecules to the TiO_2 catalyst, the reaction kinetics should depend greatly on the electron transfer efficiency. It is found that a thin alumina overlayer formed on the surface of TiO_2 by modification. The interaction between dye RhB and aluminum-modified TiO_2, as explored by IR spectra, diffuse reflectance, and the fluorescence emission spectra, is stronger than that between RhB and TiO_2, which implies the predominant adsorption of dye RhB on the Al_2O_3 overlayer. This Al_2O_3 layer intervened between dye and TiO_2 would inevitably influence the electron transfer from excited dye to TiO_2 under visible irradiation. As indicated previously (*13–16*) in the research of dye-sensitized solar cell, the metal oxide overlayer, especially the Al_2O_3, acts as a barrier layer between electron donor and acceptor, and thus inhibits electron back transfer from semiconductor to the redox electrolyte. The tunneling electron injection from the excited dye molecule into the conduction band of TiO_2 is suppressed to a much less extent by the thin insulating Al_2O_3 layer (*16*). The increase in photovoltage and overall efficiency are ascribed to retardation of this charge recombination loss. In our system, the Al_2O_3 insulating layer intervened between dye and TiO_2, should function in a similar manner to slow the recombination between injected electrons and dye cations and result in the enhanced photodegradation of dye pollutants under visible irradiation. On the other hand, the modification seems not to hinder the capture of conduction band electron by O_2 absorbed on the surface of catalyst, and the formation of active radical species, such as $HOO^{\bullet}$ and $HO^{\bullet}$ (Figure S9).

Acknowledgments

The generous financial support by the Ministry of Science and Technology of China (2003CB415006), by the National Science Foundation of China (20537010, 20520120221, and 50436040), and the Chinese Academy of Sciences is gratefully acknowledged.

Supporting Information Available

HPLC analysis of the products; the stability experiment of the modified catalyst; O1s and Al2p XPS spectra of the pure

Al_2O_3; ξ-potential measurement; UV–vis diffuse reflectance spectra; the normalized absorption and fluorescence emission spectra of dye RhB in aqueous solution, adsorbed on pure TiO_2, Al_2O_3, and TiO_2 (0.10Al)); the calculated orbital distribution of the HOMO and LUMO for the RhB dye and its cationic radical; the ESR spectra for superoxide radical and hydroxyl radical adducts and some discussion on these results. This material is available free of charge via the Internet at http://pubs.acs.org.

Literature Cited

(1) Wu, T. X.; Liu, G. M.; Zhao, J. C.; Hidaka, H.; Serpone, N. Photoassisted degradation of dye pollutants. V. Self-photosensitized oxidative transformation of Rhodamine B under visible light irradiation in aqueous TiO_2 dispersions. *J. Phys. Chem. B* **1998**, *102*, 5845.

(2) Zhang, F. L.; Zhao, J. C.; Shen, T.; Hidaka, H.; Pelizzetti, E.; Serpone, N. TiO_2-assisted photodegradation of dye pollutants II. Adsorption and degradation kinetics of eosin in TiO_2 dispersions under visible light irradiation. *Appl. Catal., B* **1998**, *15*, 147.

(3) Liu, G. M.; Wu, T. X.; Zhao, J. C.; Hidaka, H.; Serpone, N. Photoassisted degradation of dye pollutants. 8. Irreversible degradation of alizarin red under visible light radiation in air-equilibrated aqueous TiO_2 dispersions. *Environ. Sci. Technol.* **1999**, *33*, 2081.

(4) Vinodgopal, K.; Wynkoop, D. E.; Kamat, P. V. Environmental photochemistry on semiconductor surfaces: photosensitized degradation of a textile azo dye, Acid Orange 7, on TiO_2 particles using visible light. *Environ. Sci. Technol.* **1996**, *30*, 1660.

(5) Kyung, H.; Lee, J.; Choi, W. Simultaneous and synergistic conversion of dyes and heavy metal ions in aqueous TiO_2 suspensions under visible-light illumination. *Environ. Sci. Technol.* **2005**, *39*, 2376.

(6) Zhao, J. C.; Wu, T. X.; Wu, K. Q.; Oikawa, K.; Hidaka, H.; Serpone, N. Photoassisted degradation of dye pollutants. 3. Degradation of the cationic dye rhodamine B in aqueous anionic surfactant/TiO_2 dispersions under visible light irradiation: Evidence for the need of substrate adsorption on TiO_2 particles. *Environ. Sci. Technol.* **1998**, *32*, 2394.

(7) Tincher, W. C. Processing wastewater from carpet mills. *Text. Chem. Color* **1989**, *21*, 33.

(8) Ganesh, R.; Boardman, G. D.; Michelsen, D. Fate of azo dyes in sludges. *Water Res.* **1994**, *28*, 1367.

(9) Weber, E. J.; Adams, R. L. Chemical- and sediment-mediated reduction of the azo dye disperse Blue 79. *Environ. Sci. Technol.* **1995**, *29*, 1163.

(10) Franch, M. I.; Peral, J.; Domènech, X.; Howe, R. F.; Ayllón, J. A. Enhancement of photocatalytic activity of TiO_2 by adsorbed aluminum(III). *Appl. Catal., B* **2005**, *55*, 105–113.

(11) Gesenhues, U. Al-doped TiO_2 pigments: influence of doping on the photocatalytic degradation of alkyd resins. *J. Photochem. Photobiol., A* **2001**, *139*, 243–251.

(12) Anderson, C.; Bard, A. J. Improved photocatalytic activity and characterization of mixed TiO_2/SiO_2 and TiO_2/Al_2O_3 materials. *J. Phys. Chem. B* **1997**, *101*, 2611.

(13) Alarcon, H.; Boschloo, G.; Mendoza, P.; Solis, J. L.; Hagfeldt, A. Dye-sensitized solar cells based on nanocrystalline TiO_2 films surface treated with Al^{3+} ions: Photovoltage and electron transport studies. *J. Phys. Chem. B* **2005**, *109*, 18483.

(14) Palomares, E.; Clifford, J. N.; Haque, S. A.; Lutz, T.; Durrant, J. R. Slow charge recombination in dye-sensitised solar cells (DSSC) using Al_2O_3 coated nanoporous TiO_2 films. *Chem. Commun.* **2002**, 1464.

(15) Durrant, J. R.; Haque, S. A.; Palomares, E. Photochemical energy conversion: from molecular dyads to solar cells. *Chem. Commun.* **2006**, 3279.

(16) Palomares, E.; Clifford, J. N.; Haque, S. A.; Lutz, T.; Durrant, J. R. Control of charge recombination dynamics in dye sensitized solar cells by the use of conformally deposited metal oxide blocking layers. *J. Am. Chem. Soc.* **2003**, *125*, 475.

(17) Anderson, N. A.; Lian, T. Ultrafast electron transfer at the molecule-semiconductor nanoparticle interface. *Annu. Rev. Phys. Chem.* **2005**, *56*, 491.

(18) Watson, D. F.; Meyer, G. J. Electron injection at dye-sensitized semiconductor electrodes. *Annu. Rev. Phys. Chem.* **2005**, *56*, 119.

(19) Tachibana, Y.; Haque, S. A.; Mercer, I. P.; Moser, J. E.; Klug, D. R.; Durrant, J. R. Modulation of the rate of electron injection in dye-sensitized nanocrystalline TiO_2 films by externally applied bias. *J. Phys. Chem. B* **2001**, *105*, 7424.

(20) Anderson, N. A.; Ai, X.; Chen, D. T.; Mohler, D. L.; Lian, T. Q. Bridge-assisted ultrafast interfacial electron transfer to nanocrystalline SnO_2 thin films. *J. Phys. Chem. B* **2003**, *107*, 14231.

(21) Clifford, J. N.; Palomares, E.; Nazeeruddin, M. K.; Gratzel, M.; Nelson, J.; Li, X.; Long, N. J.; Durrant, J. R. Molecular control of recombination dynamics in dye-sensitized nanocrystalline TiO_2 films: Free energy vs distance dependence. *J. Am. Chem. Soc.* **2004**, *126*, 5225.

(22) Ruiz, A. M.; Dezanneau, G.; Arbiol, J.; Cornet, A.; Morante, J. R. Insights into the structural and chemical modifications of Nb additive on TiO_2 nanoparticles. *Chem. Mater.* **2004**, *16*, 862.

(23) Bourikas, K.; Stylidi, M.; Kondarides, D. I.; Verykios, X. E. Adsorption of Acid Orange 7 on the surface of titanium dioxide. *Langmuir* **2005**, *21*, 9222.

(24) Chen, C. C.; Zhao, W.; Lei, P. X.; Zhao, J. C.; Serpone, N. Photosensitized degradation of dyes in polyoxometalate solutions versus TiO_2 dispersions under visible-light irradiation: Mechanistic implications. *Chem. Eur. J.* **2004**, *10*, 1956.

(25) Liu, G. M.; Li, X. Z.; Zhao, J. C.; Hidaka, H.; Serpone, N. Photooxidation pathway of sulforhodamine-B. Dependence on the adsorption mode on TiO_2 exposed to visible light radiation. *Environ. Sci. Technol.* **2000**, *34*, 3982.

(26) Li, X. Z.; Liu, G. M.; Zhao, J. C. Two competitive primary processes in the photodegradation of cationic triarylmethane dyes under visible irradiation in TiO_2 dispersions. *New J. Chem.* **1999**, *23*, 1193.

(27) Zhao, W.; Chen, C. C.; Li, X. Z.; Zhao, J. C.; Hidaka, H.; Serpone, N. Photodegradation of Sulforhodamine-B dye in platinized titania dispersions under visible light irradiation: Influence of platinum as a functional co-catalyst. *J. Phys. Chem. B* **2002**, *106*, 5022.

(28) Hoertz, P. G.; Staniszewski, A.; Marton, A.; Higgins, G. T.; Incarvito, C. D.; Rheingold, A. L.; Meyer, G. J. Toward exceeding the Shockley−Queisser limit: Photoinduced interfacial charge transfer processes that store energy in excess of the equilibrated excited state. *J. Am. Chem. Soc.* **2006**, *128*, 8234.

(29) Tannenbaum, R.; King, S.; Lecy, J.; Tirrell, M.; Potts, L. Infrared study of the kinetics and mechanism of adsorption of acrylic polymers on alumina surfaces. *Langmuir* **2004**, *20*, 4507.

(30) Shklover, V.; Nazeeruddin, M. K.; Zakeeruddin, S. M.; Barbe, C.; Kay, A.; Haibach, T.; Steurer, W.; Hermann, R.; Nissen, H. U.; Gratzel, M. Structure of nanocrystalline TiO_2 powders and precursor to their highly efficient photosensitizer. *Chem. Mater.* **1997**, *9*, 430.

(31) David, R. L. *CRC Handbook of Chemistry and Physics*; CRC Press: Boca Raton, FL, 2005.

(32) Baumann, T. F.; Gash, A. E.; Chinn, S. C.; Sawvel, A. M.; Maxwell, R. S.; Satcher, J. H. Synthesis of high-surface-area alumina aerogels without the use of alkoxide precursors. *Chem. Mater.* **2005**, *17*, 395.

(33) Miller, J. M.; Lakshmi, L. J. Spectroscopic characterization of sol-gel-derived mixed oxides. *J. Phys. Chem. B* **1998**, *102*, 6465.

(34) Fitzgerald, J. J.; Piedra, G.; Dec, S. F.; Seger, M.; Maciel, G. E. Dehydration studies of a high-surface-area alumina (pseudoboehmite) using solid-state ^1H and ^{27}Al NMR. *J. Am. Chem. Soc.* **1997**, *119*, 7832.

(35) Wouters, B. H.; Chen, T.; Goossens, A. M.; Martens, J. A.; Grobet, P. J. Determination of the Al^{T1}/Al^{T2} aatio in MAZ zeolites using line shapes of MQ MAS NMR. *J. Phys. Chem. B* **1999**, *103*, 8093.

(36) Fu, X.; Clark, L. A.; Yang, Q.; Anderson, M. A. Enhanced photcatalytic performance of titania-based binary metal oxides: TiO_2-SiO_2 and TiO_2-ZrO_2. *Environ. Sci. Technol.* **1996**, *30*, 647.

(37) Galán-Ferers, M.; Alemany, L. J.; Mariscal, R.; Bañares, M. A.; Anderson, J. A.; Fierro, J. L. G. Surface acidity and properties of titania-silica catalysts. *Chem. Mater.* **1995**, *7*, 1342.

(38) Tanabe, K.; Sumiyoshi, T.; Shibita, T.; Kiyoura, T.; Kitagawa. A new hypothesis regarding the surface acidity of binary metal oxides. *J. Bull. Chem. Soc. Jpn.* **1974**, *47*, 1064.

(39) Pan, J. H.; Lee, W. I. Preparation of highly ordered cubic mesoporous WO_3/TiO_2 films and their photocatalytic properties. *Chem. Mater.* **2006**, *18*, 847.

(40) Finnie, K. S.; Bartlett, J. R.; Woolfrey, J. L. Vibrational spectroscopic study of the coordination of (2,2′-bipyridyl-4,4′-dicarboxylic acid)ruthenium(II) complexes to the surface of nanocrystalline titania. *Langmuir* **1998**, *14*, 2744.

(41) Weng, Y. X.; Li, L.; Liu, Y.; Wang, L.; Yang, G. Z. Surface-binding forms of carboxylic groups on nanoparticulate TiO_2 surface studied by the interface-sensitive transient triplet-state molecular probe. *J. Phys. Chem. B* **2003**, *107*, 4356.

(42) Boettcher, S. W.; Bartl, M. H.; Hu, J. G.; Stucky, G. D. Structural analysis of hybrid titania-based mesostructured composites. *J. Am. Chem. Soc.* **2005**, *127*, 9721.
(43) Deacon, G. B.; Phillips, R. J. Relationships between the carbon-oxygen stretching frequencies of carboxylato complexes and the type of carboxylate coordination. *Coord. Chem. Rev.* **1980**, *33*, 227.
(44) Couzis, A.; Gulari, E. Adsorption of sodium laurate from its aqueous solution onto an alumina surface. A dynamic study of the surface-surfactant interaction using attenuated total reflection Fourier transform infrared spectroscopy. *Langmuir* **1993**, *9*, 3414.
(45) Nara, M.; Torri, H.; Tasumi, M. Correlation between the vibrational frequencies of the carboxylate group and the types of its coordination to a metal ion: An ab initio molecular orbital study. *J. Phys. Chem.* **1996**, *100*, 19812.

ES071770E